

A comparison of different order hybrid finite difference-volume methods for solving the Serre equations in conservative law form

Jordan Pitt,¹
Christopher Zoppou,¹
Stephen G. Roberts,¹

ABSTRACT

In this paper we describe first- to third-order accurate numerical methods for solving the Serre equations. These methods are described as finite difference- finite volume methods because they use a finite difference approximation and a finite volume method to solve the Serre equations in conservation law form. These models are validated and used to investigate a conjecture in the literature about the results of solving the Serre equations in the presence of steep gradients. To adequately resolve dispersive waves efficiently in problems containing steep gradients a scheme is required to be at least second-order accurate.

Keywords: dispersive waves, conservation laws, Serre equations, finite volume method, finite difference method

¹ INTRODUCTION

Free surface flows occur in many important applications such as: tsunamis, storm surges and tidal bores. Because fluid viscosity has a negligible effect on these problems they can be modelled by the Euler equations. However, numerical methods for the Euler equations are computationally expensive when dealing with these problems over large domains. Thus various approximations to the Euler equations have been derived; one of the crudest is the shallow water wave (SWW) equations which have been used to model free surface flows in the past. However, the SWW equations assume a hydrostatic pressure distribution in a fluid column which is not fully justified in rapidly varying flows where

¹Mathematical Sciences Institute, Australian National University, Canberra, ACT 0200, Australia, E-mail: Jordan.Pitt@anu.edu.au. The work undertaken by the first author was supported financially by an Australian National University Scholarship.

10 vertical acceleration of the fluid particles becomes important. It is the vertical acceleration
11 of these particles that produces a non-hydrostatic pressure distribution and dispersive
12 waves which are not present in the SWW equations. Consequently, many equations have
13 been derived as approximations to the Euler equations in shallow fluids that are less re-
14 strictive in their assumptions than the SWW equations. The Serre equations are one of
15 these approximations to the Euler equations and are of particular interest because they
16 do not enforce a hydrostatic pressure distribution over a fluid column allowing for fully
17 non-linear and weakly dispersive shallow water flows (Lannes and Bonneton 2009).

18 The Serre equations were first derived by Serre (1953) for flat bottom topographies in
19 one dimension. More general equations were then derived for smooth bottom topographies
20 in one dimension (Su and Gardner 1969) and later smooth bottom topographies in two di-
21 mensions (Green and Naghdi 1976). These equations have been handled in many different
22 ways (Mitsotakis et al. 2014; Bonneton et al. 2011; Antunes do Carmo et al. 1993; Chazel
23 et al. 2011; Cienfuegos and Bonneton 2006; Cienfuegos and Bonneton 2007; Dutykh et al.
24 2011). This paper follows the decomposition of the Serre equations into conservative law
25 form (Le Métayer et al. 2010; Li et al. 2014; Zoppou 2014) and follows the formulation
26 of Le Métayer et al. (2010) and Zoppou (2014). First-, second- and third-order accurate
27 numerical methods are developed for solving the Serre equations in conservation law form.

28 This paper aims to clear up the discrepancy between the results of Le Métayer et al.
29 (2010) and El et al. (2006) by examining the behaviour of a certain dam-break problem.
30 In particular, Le Métayer et al. (2010) stated that their first-order method was sufficient to
31 capture the important behaviour of the dam-break problem; this paper will test the validity
32 of that assertion. To accomplish this first-, second- and third-order accurate methods to
33 solve the Serre equations are constructed and validated by comparing the solutions to a
34 known analytical solution to the Serre equations and laboratory data of flows containing
35 steep gradients. The validated models supported the findings of El et al. (2006).

36 SERRE EQUATIONS

37 The Serre equations can be derived by integrating the Euler equations over the water
38 depth, as was done by Su and Gardner (1969). They can also be derived from an asymptotic
39 expansion of the Euler equations (Lannes and Bonneton 2009). The former is more
40 consistent with the perspective from which numerical methods will be developed in this
41 paper while the latter is useful for identifying the appropriate regions in which to use these
42 equations as a model of fluid flow.

43 The scenario under which the Serre approximation is made consists of a two dimen-
44 sional $\mathbf{x} = (x, z)$ fluid over a variable bathymetry as in Figure 1, under the action of
45 gravity. The water depth is $h(x, t)$ and $z_b(x)$ is the bed elevation. The fluid is subject
46 to the pressure, $p(\mathbf{x}, t)$ and gravitational acceleration, $\mathbf{g} = (0, g)^T$ and has a velocity
47 $\mathbf{v} = (u(\mathbf{x}, t), w(\mathbf{x}, t))$, where $u(\mathbf{x}, t)$ is the velocity in the x -coordinate and $w(\mathbf{x}, t)$ is the

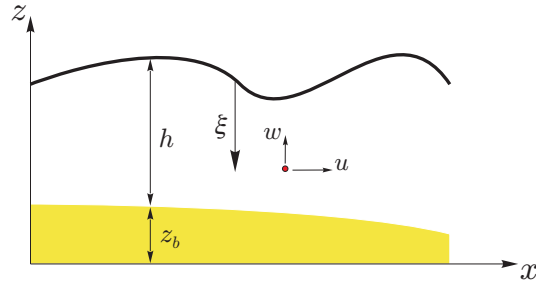


FIG. 1: The notation used for one-dimensional flow governed by the Serre equation.

48 velocity in the z -coordinate and t is time. Assuming that $z_b(x)$ is constant the Serre equa-
 49 tions read (Li et al. 2014; Zoppou 2014)

50 51 52

$$\frac{\partial h}{\partial t} + \frac{\partial(\bar{u}h)}{\partial x} = 0, \quad (1a)$$

53

$$\underbrace{\frac{\partial(\bar{u}h)}{\partial t} + \frac{\partial}{\partial x} \left(\bar{u}^2 h + \frac{gh^2}{2} \right)}_{\text{Shallow Water Wave Equations}} + \underbrace{\frac{\partial}{\partial x} \left(\frac{h^3}{3} \left[\frac{\partial \bar{u}}{\partial x} \frac{\partial \bar{u}}{\partial x} - \bar{u} \frac{\partial^2 \bar{u}}{\partial x^2} - \frac{\partial^2 \bar{u}}{\partial x \partial t} \right] \right)}_{\text{Dispersion Terms}} = 0 \quad (1b)$$

54

$$\underbrace{\quad}_{\text{Serre Equations}}$$

55 where \bar{u} is the depth averaged velocity.

56 **Alternative Conservation Law Form of the Serre Equations**

57 In Le Métayer et al. (2010) and Zoppou (2014) it is demonstrated that the Serre equa-
 58 tions can be rearranged into a conservation law form, by introducing a new conserved
 59 quantity

60 61

$$G = uh - h^2 \frac{\partial h}{\partial x} \frac{\partial u}{\partial x} - \frac{h^3}{3} \frac{\partial^2 u}{\partial x^2}. \quad (2)$$

62 Consequently, (1) can be rewritten as

63 64

$$\frac{\partial h}{\partial t} + \frac{\partial(uh)}{\partial x} = 0 \quad (3a)$$

65 and

66 67

$$\frac{\partial G}{\partial t} + \frac{\partial}{\partial x} \left(Gu + \frac{gh^2}{2} - \frac{2h^3}{3} \frac{\partial u}{\partial x} \frac{\partial u}{\partial x} \right) = 0 \quad (3b)$$

68 where the bar over u has been dropped to simplify the notation. A hybrid method can be
 69 developed for the Serre equations that solves the elliptic problem (2) for u and then the
 70 conservation law (3) for h and G . This replicates the process of Le Métayer et al. (2010)
 71 and Zoppou (2014).

72 NUMERICALLY SOLVING THE SERRE EQUATIONS WRITTEN IN 73 CONSERVATION LAW FORM

74 There are numerous ways a numerical method could be built to solve the Serre equa-
 75 tions in conservation law form (3). For flows that contain steep gradients the finite volume
 76 method seems the most appropriate. A finite volume method to solve (3) updates the
 77 conserved quantities h and G over a single time step $\Delta t = t^{n+1} - t^n$. So that

$$78 \quad \begin{bmatrix} h^{n+1} \\ G^{n+1} \end{bmatrix} = \mathcal{L}(h^n, G^n, u^n, \Delta t) \quad (4)$$

80 where \mathcal{L} is some numerical solver for (3) and the superscript denotes the time at which a
 81 quantity is evaluated; e.g. $u^n = u(t^n)$. The complete solution also involves solving (2) for
 82 u given h and G denoted by

$$83 \quad u^{n+1} = \mathcal{A}(h^{n+1}, G^{n+1}). \quad (5)$$

85

86 SOLVING THE ELLIPTIC EQUATION \mathcal{A} FOR U

87 Assuming that a discretisation in space has a fixed resolution so that $x_{i+1} - x_i = \Delta x$
 88 for all i ; allows for a simple finite difference approximation to (2) as a suitable method
 89 for \mathcal{A} (Le Métayer et al. 2010; Zoppou 2014). Since the goal of this paper is to develop
 90 and compare a range of different order accurate methods for this problem both a second-
 91 and fourth-order centred finite difference approximation to (2) were used. By taking such
 92 approximations to the first- and second-order spatial derivatives the second- and fourth-
 93 order analogues of (2) are given by

$$94 \quad G_i = u_i h_i - h_i^2 \left(\frac{h_{i+1} - h_{i-1}}{2\Delta x} \right) \left(\frac{u_{i+1} - u_{i-1}}{2\Delta x} \right) - \frac{h_i^3}{3} \left(\frac{u_{i+1} - 2u_i + u_{i-1}}{\Delta x^2} \right) \quad (5a)$$

95 and

$$96 \quad G_i = u_i h_i - h_i^2 \left(\frac{-h_{i+2} + 8h_{i+1} - 8h_{i-1} + h_{i-2}}{12\Delta x} \right) \left(\frac{-u_{i+2} + 8u_{i+1} - 8u_{i-1} + u_{i-2}}{12\Delta x} \right) \\ 97 \quad - \frac{h_i^3}{3} \left(\frac{-u_{i+2} + 16u_{i+1} - 30u_i + 16u_{i-1} - u_{i-2}}{12\Delta x^2} \right) \quad (5b)$$

99 where the subscript denotes the spatial coordinate at which the quantity is evaluated; e.g.
100 $u_i = u(x_i)$. Both of these can be rearranged into a matrix equation with the following form

$$101 \quad \begin{bmatrix} u_0 \\ \vdots \\ u_m \end{bmatrix} = A^{-1}(h) \begin{bmatrix} G_0 \\ \vdots \\ G_m \end{bmatrix} =: \mathcal{A}(\mathbf{h}, \mathbf{G})$$

102

103 where for a second-order approximation the matrix $A(h)$ is tri-diagonal while for a fourth-
104 order method it is penta-diagonal.

105 SOLVING THE CONSERVATION LAW FORM OF THE SERRE EQUATIONS

106 A finite volume method of sufficient order was developed to solve (3). Unlike finite
107 difference methods which utilise nodal values of quantities, finite volume methods use the
108 cell averages of the conserved quantities, for example the average water depth over a cell
109 which spans $[x_{i-1/2}, x_{i+1/2}]$ is

$$110 \quad \bar{h}_i = \frac{1}{\Delta x} \int_{x_{i-\frac{1}{2}}}^{x_{i+\frac{1}{2}}} h(x, t) dx$$

111

112 where $x_{i\pm 1/2} = x_i \pm \Delta x/2$. Finite volume methods update the cell averages using

$$113 \quad \bar{U}_i^{n+1} = \bar{U}_i^n - \frac{\Delta t}{\Delta x} \left(F_{i+\frac{1}{2}}^n - F_{i-\frac{1}{2}}^n \right) \quad (6)$$

114

115 where $\bar{U}_i^n = [\bar{h}_i^n \ \bar{G}_i^n]^T$ is an approximation of the vector of the conserved quantities aver-
116 aged over the cell at time t^n . While $F_{i\pm 1/2}^n$ is an approximation of the average flux over the
117 time interval $[t^n, t^{n+1}]$ at the respective cell boundary $x_{i\pm 1/2}$, which is obtained by solving a
118 local Riemann problem at the cell boundaries.

119 Local Riemann Problem

120 Since \bar{U}_i^n is known for all i , what remains is to calculate the time averaged fluxes $F_{i\pm 1/2}$
121 in (6). In Kurganov et al. (2002) the time averaged inter-cell flux is approximated by

$$122 \quad F_{i+\frac{1}{2}} = \frac{a_{i+\frac{1}{2}}^+ f(q_{i+\frac{1}{2}}^-) - a_{i+\frac{1}{2}}^- f(q_{i+\frac{1}{2}}^+)}{a_{i+\frac{1}{2}}^+ - a_{i+\frac{1}{2}}^-} + \frac{a_{i+\frac{1}{2}}^+ a_{i+\frac{1}{2}}^-}{a_{i+\frac{1}{2}}^+ - a_{i+\frac{1}{2}}^-} \left[q_{i+\frac{1}{2}}^+ - q_{i+\frac{1}{2}}^- \right] \quad (7)$$

123

124 where f is the instantaneous flux of the conserved quantity q evaluated using the recon-
125 structed values from the cells adjacent to the cell interface $x_{i+1/2}$. While $a_{i+1/2}^-$ and $a_{i+1/2}^+$
126 are given by

$$127 \quad a_{i+\frac{1}{2}}^- = \min \left[\lambda_1 \left(q_{i+\frac{1}{2}}^- \right), \lambda_1 \left(q_{i+\frac{1}{2}}^+ \right), 0 \right]$$

128

129 and

130 $a_{i+\frac{1}{2}}^+ = \max \left[\lambda_2 \left(q_{i+\frac{1}{2}}^- \right), \lambda_2 \left(q_{i+\frac{1}{2}}^+ \right), 0 \right]$

131

132 where λ_1 and λ_2 are estimates of the smallest and largest eigenvalues respectively of the
133 Jacobian, $\partial f / \partial u$.

134 **Propagation Speeds of a Local Shock**

135 The phase speed v_p of the Serre equations can be calculated by a linearisation to be

136 $v_p = u \pm \sqrt{gh} \sqrt{\frac{3}{h^2 k^2 + 3}}$

137

138 where k is the wave number (Zoppou 2014). Thus the phase speeds of the SWW equations
139 bound the phase speeds of the Serre equations so λ_1 and λ_2 can be defined as such

140 $\lambda_1 := u - \sqrt{gh} \leq v_p \leq u + \sqrt{gh} =: \lambda_2.$

142 **Reconstruction of Conserved Quantities**

143 The quantities $q_{i+1/2}^-$ and $q_{i+1/2}^+$ in (7) are given by the two reconstructions at $x_{i+1/2}$,
144 one from the cell to the left $[x_{i-1/2}, x_{i+1/2}]$ and one from the cell to the right $[x_{i+1/2}, x_{i+3/2}]$
145 denoted by the superscripts $-$ and $+$ respectively. The order of the polynomials used to
146 reconstruct the quantities inside the cells determines the spatial order of accuracy. Constant
147 polynomials result in a first-order method (Godunov 1959). Similarly first- and second-
148 degree polynomials result in second- and third-order accurate methods respectively.

149 For a zero-degree polynomial the interpolant has the value \bar{q}_i at x_i , this is also the
150 case for linear interpolation functions. For the zero-degree case the interpolants are fully
151 determined i.e $q_{i-1/2}^+ = \bar{q}_i = q_{i+1/2}^-$ and monotinicity preserving. There are a variety of
152 ways to construct higher-degree interpolants not all of which are necessarily monotonicity
153 preserving, which can result in the introduction of numerical oscillations during the re-
154 construction process. To suppress these non-physical oscillations in higher order methods
155 limiting must be implemented. For the second-order method the minmod limiter was used
156 as in Kurganov et al. (2002). While for the third-order method the Koren limiter was used
157 (Koren 1993). This results in the following reconstruction scheme for the second-order
158 method

159 $q_{i+\frac{1}{2}}^- = \bar{q}_i + a_i \frac{\Delta x}{2}$

160

161 and

162 $q_{i+\frac{1}{2}}^+ = \bar{q}_{i+1} - a_{i+1} \frac{\Delta x}{2}$

163

164 where

$$165 \quad 166 \quad a_i = \text{minmod} \left\{ \theta \frac{\bar{q}_{i+1} - \bar{q}_i}{\Delta x}, \frac{\bar{q}_{i+1} - \bar{q}_{i-1}}{2\Delta x}, \theta \frac{\bar{q}_i - \bar{q}_{i-1}}{\Delta x} \right\} \quad \text{for } \theta \in [1, 2].$$

167 While for the third-order method the reconstruction scheme is

$$168 \quad 169 \quad q_{i+\frac{1}{2}}^- = \bar{q}_i + \frac{1}{2} \phi^-(r_i) (\bar{q}_i - \bar{q}_{i-1})$$

170 and

$$171 \quad 172 \quad q_{i+\frac{1}{2}}^+ = \bar{q}_{i+1} - \frac{1}{2} \phi^+(r_{i+1}) (\bar{q}_{i+1} - \bar{q}_i)$$

173 where

$$174 \quad 175 \quad 176 \quad \phi^-(r_i) = \max \left[0, \min \left[2r_i, \frac{1+2r_i}{3}, 2 \right] \right],$$

$$177 \quad 178 \quad \phi^+(r_i) = \max \left[0, \min \left[2r_i, \frac{2+r_i}{3}, 2 \right] \right]$$

179 and

$$180 \quad 181 \quad r_i = \frac{\bar{q}_{i+1} - \bar{q}_i}{\bar{q}_i - \bar{q}_{i-1}}.$$

182 Reconstruction of u

183 The finite difference methods for (5) return u as nodal values at the cell centres thus the
 184 reconstruction of u at the cell edges is different to the process described above for h and G .
 185 Assuming u is smooth a simple interpolation can be used without limiting. For first- and
 186 second-order methods the linear interpolation between the two neighbouring cell centres
 187 was used which results in the cell edge value being the average of the two neighbouring
 188 cell centre values. For the third-order method the cubic that interpolates the 4 neighbouring
 189 cell centres was used. This resulted in the following for first- and second-order

$$190 \quad 191 \quad u_{i+\frac{1}{2}} = \frac{u_{i+1} + u_i}{2}$$

192 and for third-order

$$193 \quad 194 \quad u_{i+\frac{1}{2}} = \frac{-3u_{j+2} + 27u_{j+1} + 27u_j - 3u_{j-1}}{48}.$$

195 **Fully discrete approximations to the instantaneous flux $f(q_{i+\frac{1}{2}}^\pm)$**

196 For water depth, the fully discrete approximation to $f(h_{i+1/2}^\pm)$ in (3a) is given by

197 198
$$f\left(h_{i+\frac{1}{2}}^\pm\right) = u_{i+\frac{1}{2}}^\pm h_{i+\frac{1}{2}}^\pm$$

199 which is independent of the order of accuracy of the method.

200 201 The flux $f(G_{i+1/2}^\pm)$ is more complicated because of the derivative term in (3b) and is given by

202 203
$$f\left(G_{i+\frac{1}{2}}^\pm\right) = u_{i+\frac{1}{2}}^\pm G_{i+\frac{1}{2}}^\pm + \frac{g}{2} \left(h_{i+\frac{1}{2}}^\pm\right)^2 - \frac{2}{3} \left(h_{i+\frac{1}{2}}^\pm\right)^3 \left[\left(\frac{\partial u}{\partial x}\right)_{i+\frac{1}{2}}\right]^2.$$

204 The first-, second- and third-order approximations to the derivative term can be obtained by
205 taking the derivative of the interpolating polynomial used in the reconstruction of u . Thus
206 the following approximations to the derivatives were obtained, for the first- and second-
207 order method

208 209
$$\left(\frac{\partial u}{\partial x}\right)_{i+\frac{1}{2}} = \frac{u_{i+1} - u_i}{\Delta x}$$

210 and for the third-order method

211 212
$$\left(\frac{\partial u}{\partial x}\right)_{i+\frac{1}{2}} = \frac{-u_{i+2} + 27u_{i+1} - 27u_i + u_{i-1}}{24\Delta x}.$$

213 **Transforming between nodal values and cell averages**

214 215 The operator \mathcal{L} given by (6) uses cell averages while the operator \mathcal{A} given by (5a)
216 and (5b) uses nodal values at the cell centres. Therefore, a transformation from the cell
217 averages to the nodal values is required. For the first- and second-order methods this
218 distinction is trivial since $\bar{q}_i = q_i$. However, for the third-order method this is a very
219 important distinction and failure to handle this correctly will result in a loss of accuracy.

220 221 A quadratic polynomial that gives the correct cell averages for the cell centred at x_i
222 and its two neighbours satisfies this equation

221 222
$$q_i = \frac{-\bar{q}_{i+1} + 26\bar{q}_i - \bar{q}_{i-1}}{24}.$$

223 This is a tri-diagonal matrix equation that transforms from cell averages to nodal values
224 with third-order accuracy and is denoted by \mathcal{M} . The inverse transformation \mathcal{M}^{-1} denotes

225 the solution of the tri-diagonal matrix equation given nodal values resulting in cell aver-
 226 ages which is also third-order accurate. For the first- and second-order schemes \mathcal{M} is the
 227 identity matrix. This completes the solution of the Serre equations (2) and (3) with the
 228 following process denoted by \mathcal{H}

$$229 \quad \mathcal{H}(\bar{\mathbf{U}}^n, \Delta t) = \begin{cases} \mathbf{U}^n &= \mathcal{M}(\bar{\mathbf{U}}^n) \\ \mathbf{u}^n &= \mathcal{A}(\mathbf{U}^n) \\ \bar{\mathbf{U}}^{n+1} &= \mathcal{L}(\bar{\mathbf{U}}^n, \mathbf{u}^n, \Delta t) \end{cases}.$$

230

231 Strong-Stability-Preserving Runge-Kutta Scheme

232 The process above is first-order accurate in time. This paper will use the strong sta-
 233 bility Runge-Kutta steps described in Gottlieb et al. (2009) to construct fully second- and
 234 third-order accurate methods using linear combinations of \mathcal{H} . This leads to the following
 235 processes, for the first-order method

$$236 \quad \bar{\mathbf{U}}^{n+1} = \mathcal{H}(\bar{\mathbf{U}}^n, \Delta t)$$

237

238 the second-order method

$$239 \quad \bar{\mathbf{U}}^{(1)} = \mathcal{H}(\bar{\mathbf{U}}^n, \Delta t),$$

240

$$\bar{\mathbf{U}}^{(2)} = \mathcal{H}(\bar{\mathbf{U}}^{(1)}, \Delta t),$$

241

$$\bar{\mathbf{U}}^{n+1} = \frac{1}{2}(\bar{\mathbf{U}}^{(1)} + \bar{\mathbf{U}}^{(2)})$$

242

243 and the third-order method

$$244 \quad \bar{\mathbf{U}}^{(1)} = \mathcal{H}(\bar{\mathbf{U}}^n, \Delta t),$$

245

$$\bar{\mathbf{U}}^{(2)} = \mathcal{H}(\bar{\mathbf{U}}^{(1)}, \Delta t),$$

246

$$\bar{\mathbf{U}}^{(3)} = \frac{3}{4}\bar{\mathbf{U}}^n + \frac{1}{4}\bar{\mathbf{U}}^{(2)},$$

247

$$\bar{\mathbf{U}}^{(4)} = \mathcal{H}(\bar{\mathbf{U}}^{(3)}, \Delta t),$$

248

$$\bar{\mathbf{U}}^{n+1} = \frac{1}{3}\bar{\mathbf{U}}^n + \frac{2}{3}\bar{\mathbf{U}}^{(4)}.$$

249

250 Stability Constraint

251 A necessary condition for stability of all these explicit methods based on the finite
 252 volume method is the Courant-Friedrichs-Lowy condition (Courant et al. 1928) which
 253 states that for each cell

$$254 \quad \Delta t < \frac{\Delta x}{2 \max(|\lambda_i|)} \forall i. \tag{8}$$

255

256

257 **NUMERICAL SIMULATIONS**

258 We now use these methods to solve three different problems; (i) the soliton which is
 259 an analytic solution of the Serre equations; (ii) one of the experiments conducted by Ham-
 260 mack and Segur (1978) and (iii) a dam-break problem from El et al. (2006) and Le Métayer
 261 et al. (2010). The first two will be used to validate the models, with the soliton used to
 262 confirm the order of convergence of the models. The second problem is used to validate
 263 the models using experimental data which contains flows with steep gradients. Lastly the
 264 dam-break problem will be used to compare the results of these methods with those of El
 265 et al. (2006) and Le Métayer et al. (2010). The aim of which is to verify the claim of the
 266 latter that a first-order method for the Serre equations is sufficiently accurate to capture the
 267 important behaviour of the dam-break problem.

268 **Soliton**

269 Currently cnoidal waves are the only family of analytic solutions to the Serre equa-
 270 tions (Carter and Cienfuegos 2011). Solitons are a particular instance of cnoidal waves
 271 that travel without deformation and have been used to verify the convergence rates of the
 272 proposed methods in this paper.

273 For the Serre equations the solitons have the following form

$$h(x, t) = a_0 + a_1 \operatorname{sech}^2(\kappa(x - ct)) \quad (9a)$$

274 and

$$u(x, t) = c \left(1 - \frac{a_0}{h(x, t)} \right) \quad (9b)$$

275 where

$$\kappa = \frac{\sqrt{3a_1}}{2a_0 \sqrt{a_0 + a_1}} \quad (9c)$$

276 and

$$c = \sqrt{g(a_0 + a_1)} \quad (9d)$$

277 where a_0 and a_1 are input parameters that determine the depth of the quiescent water and
 278 the maximum height of the soliton above that respectively. In the simulation $a_0 = 10\text{m}$,
 279 $a_1 = 1\text{m}$ for $x \in [-500\text{m}, 1000\text{m}]$ and $t \in [0\text{s}, 50\text{s}]$. With $\Delta t = 0.5\Delta x / \sqrt{g(a_0 + a_1)}$ which
 280 satisfies (8) and $\theta = 1.2$ for the second-order reconstruction. The example results for
 281 $\Delta x = 100/2^6\text{m}$ can be seen in Figure 2.

282 Figure 2 demonstrates the superiority of the second- and third-order methods compared
 283 to the first-order method. With the first-order method there is significant attenuation of the

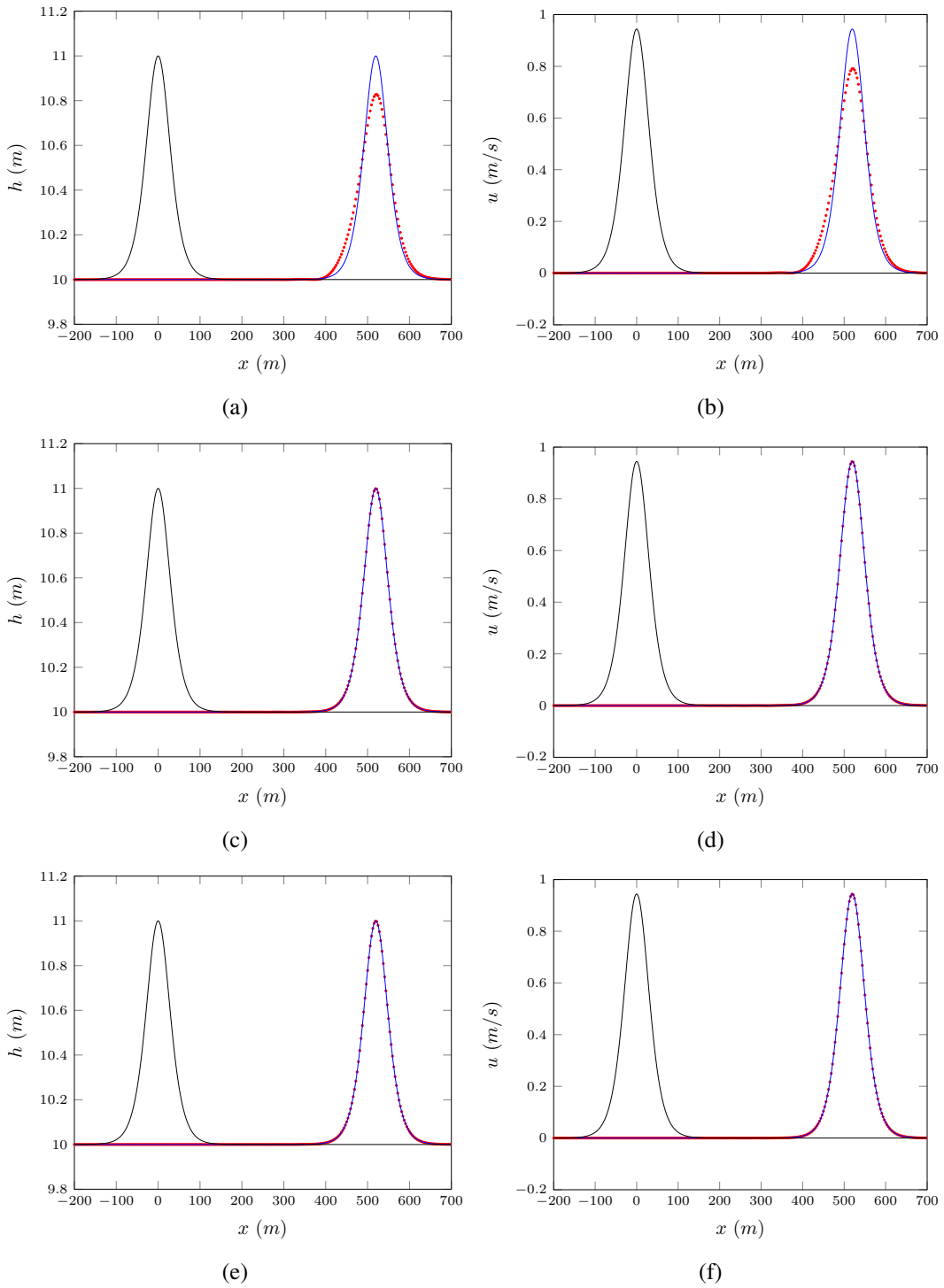


FIG. 2: The first-, second- and third-order simulation of a soliton with $\Delta x = 100/2^6$ m (\bullet) plotted against the analytic solution of (9) (—) with black for $t = 0$ s and blue for $t = 30$ s.

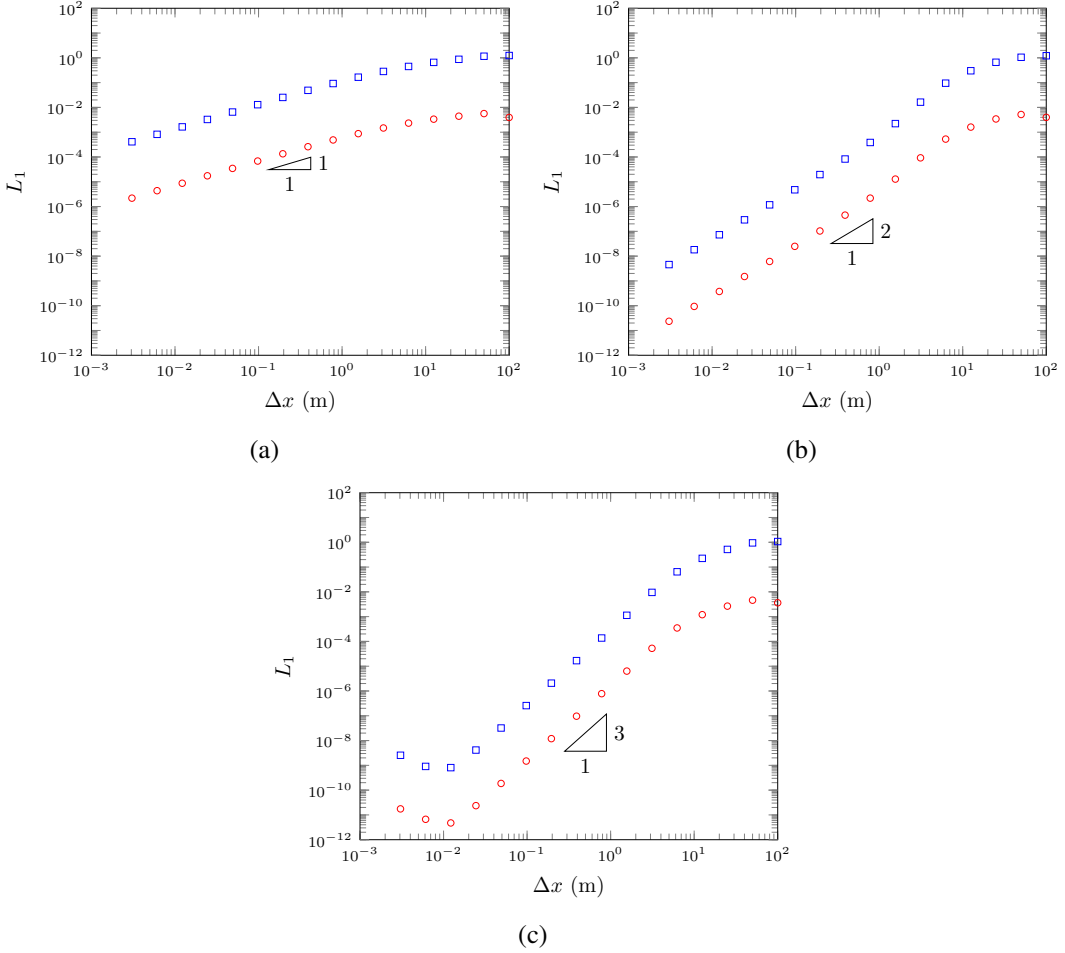


FIG. 3: Convergence of relative error using L_1 norm for analytic soliton solution for both h (\circ) and u (\diamond) for the; (a) first-, (b) second- and (c) third-order methods.

wave due to its diffusive behaviour which creates a wider wave profile and some smaller trailing waves. However, the first-order method does produce the correct speed of the wave with a small phase error. While the second- and third-order methods demonstrate no noticeable deformation resolving the soliton solution well on a relatively coarse grid with less than 500 cells defining the actual wave.

The relative error as measured by the L_1 -norm of the method can be seen in Figure 3. For a vector q and an approximation to it q^* the relative error as measured by the L_1 -norm

Order	Δx (m)	L_1 relative error for h	L_1 relative error for u	Run Time (s)
First	$100/2^{10}$	$6.85562687971 \times 10^{-5}$	$1.28856345502 \times 10^{-2}$	15.2193582058
Second	$100/2^6$	$1.28206207795 \times 10^{-5}$	$2.21972914623 \times 10^{-3}$	0.14813709259
Third	$100/2^5$	$5.27876968928 \times 10^{-5}$	$9.51078676559, \times 10^{-3}$	0.0947360992432

TABLE 1: Comparison of run times for different order methods to get similar relative error as measured by the L_1 norm for h

291 is

$$292 \quad L_1(\mathbf{q}, \mathbf{q}^*) = \frac{\sum_{i=1}^m |q_i - q_i^*|}{\sum_{i=1}^m |q_i|}. \\ 293$$

294 Figure 3 demonstrates that the methods all have the correct order of convergence in
 295 both time and space. However, this order of convergence is not uniform over all Δx . When
 296 Δx is large the actual problem is not discretised well since the cells are too large to ade-
 297 quately resolve the problem; this causes the observed suboptimal rate of convergence in
 298 Figure 3. When Δx is sufficiently small the numerical errors become small enough that
 299 floating point errors are significant and this can also lead to suboptimal rates of conver-
 300 gence as can be seen for the third-order method in Figure 3(c). Therefore, the order of
 301 convergence for all methods is confirmed.

302 Figure 3 also demonstrates the superiority of the second- and third-order methods over
 303 the first-order method for accuracy. The third-order method is also better than the second-
 304 order method in this respect although this difference is less pronounced. These differences
 305 have a significant impact on run-time if one wishes to run a simulation up to a desired
 306 accuracy. A comparison of the methods for such a problem is presented in Table 1.

307 The first-order method has a runtime two orders of magnitude greater than the second-
 308 and third-order methods. Which is reasonable because the difference in Δx is also two
 309 orders of magnitude. This is computationally restrictive as running practical problems
 310 to a reasonable accuracy can have run times that are excessive compared to second- and
 311 third-order accurate schemes. Although the second- and third-order methods are more
 312 computationally complex than the first-order method this complexity is justified if one
 313 wants to numerically solve the Serre equations up to some desired accuracy. This also
 314 demonstrates that the second-order method is adequate compared to the third-order method
 315 for solving the Serre equations up to some desired accuracy.

316 Figure 3(b) and Figure 3(c) demonstrate that the second- and third-order methods both
 317 have similar errors and Figure 2 shows that these methods resolve the problem well. There-
 318 fore, the extra effort in running a third-order method compared to a second-order method
 319 is not justified in this case. While the effort required to go from a first-order method to a

320 second-order method is justified since attaining a similar accuracy between them requires
321 a restrictively small Δx for a first-order method.

322 **Segur Laboratory Experiment**

323 Hammack and Segur (1978) conducted an experiment that produced rectangular waves
324 with the stroke of a 0.61m long piston flush with the wall of a wave tank 31.6m in length.
325 The water height was recorded at 0m, 5m, 10m, 15m and 20m from the edge of the piston
326 furthest from the wall over time. The quiescent water height h_1 was 0.1m while the stroke
327 of the piston caused a depression of water which was $h_0 = 0.095\text{m}$ deep. To run this as
328 a numerical simulation the reflected problem was used. Thus the initial conditions were
329 reflected around the origin and $h_1 - h_0$ was doubled by setting $h_0 = 0.09\text{m}$. The domain was
330 chosen to be from -60m to 60m and the simulation was for $t \in [0\text{s}, 50\text{s}]$ with $\Delta x = 0.01\text{m}$,
331 $\Delta t = 0.5\Delta x / \sqrt{gh_1}$ which satisfies (8) and $\theta = 1.2$ in the second-order scheme. The results
332 of this simulation are displayed in Figures 4 - 6.

333 In this experiment for the positive side of the axis the initial depression causes a right
334 going rarefaction fan and a left going shock. The shocks from both sides then reflect at
335 the origin and so the shock and the rarefaction fan will travel in the same direction. The
336 leading wave in all the related figures is the rarefaction fan while the trailing dispersive
337 waves are the result of the reflected shock.

338 From all the related figures it can be seen that all models show good agreement be-
339 tween the arrival of the first wave and the period of all the waves. While Figure 4 shows
340 the first-order method is too diffusive and thus under estimates the heights of the dispersive
341 waves. Whereas the second- and third-order methods over estimate them. This overesti-
342 mation can be explained by the Serre equations ignoring viscous effects that may diffuse
343 the dispersive waves and so the results could be considered as an upper bound on the wave
344 heights for non-inviscid fluids. Although even without these effects these numerical meth-
345 ods show good agreement with the experimental data thus validating them to provide a
346 reasonable representation of rapidly-varying flows. Additionally, it demonstrates that the
347 oscillations observed by the produced numerical solutions of the Serre equations around
348 steep gradients are physical and not numerical. In these simulations the numerical oscil-
349 lations that the second-order method should produce (Zoppou and Roberts 1996) do not
350 have a significant influence on the physical oscillations.

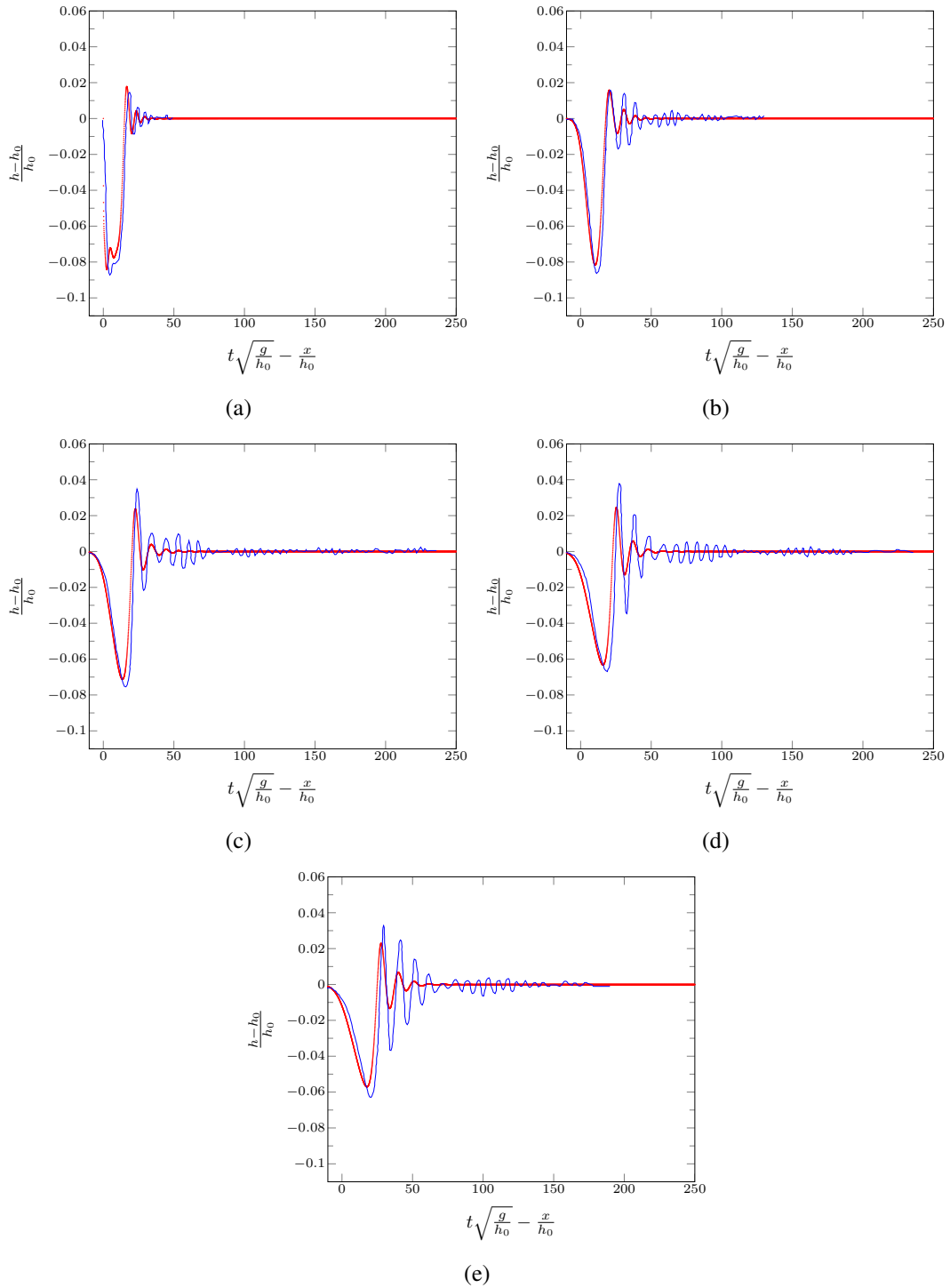


FIG. 4: Comparison of the experimental results (—) against the first-order methods solution (●) at x/h_0 : (a) 0, (b) 50, (c) 100, (d) 150 and (e) 200.

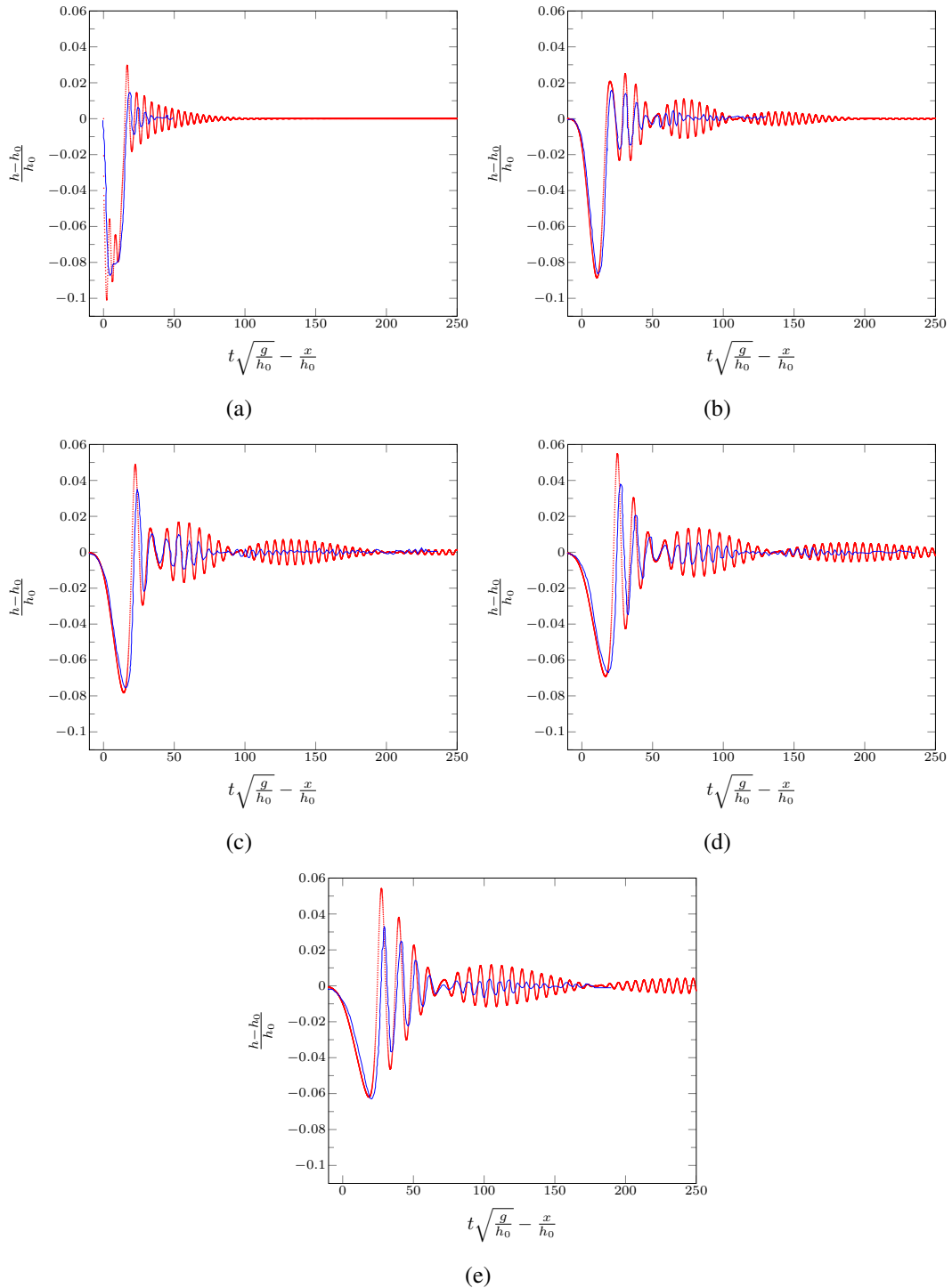


FIG. 5: Comparison of the experimental results (—) against the second-order methods solution (●) at x/h_0 : (a) 0, (b) 50, (c) 100, (d) 150 and (e) 200.

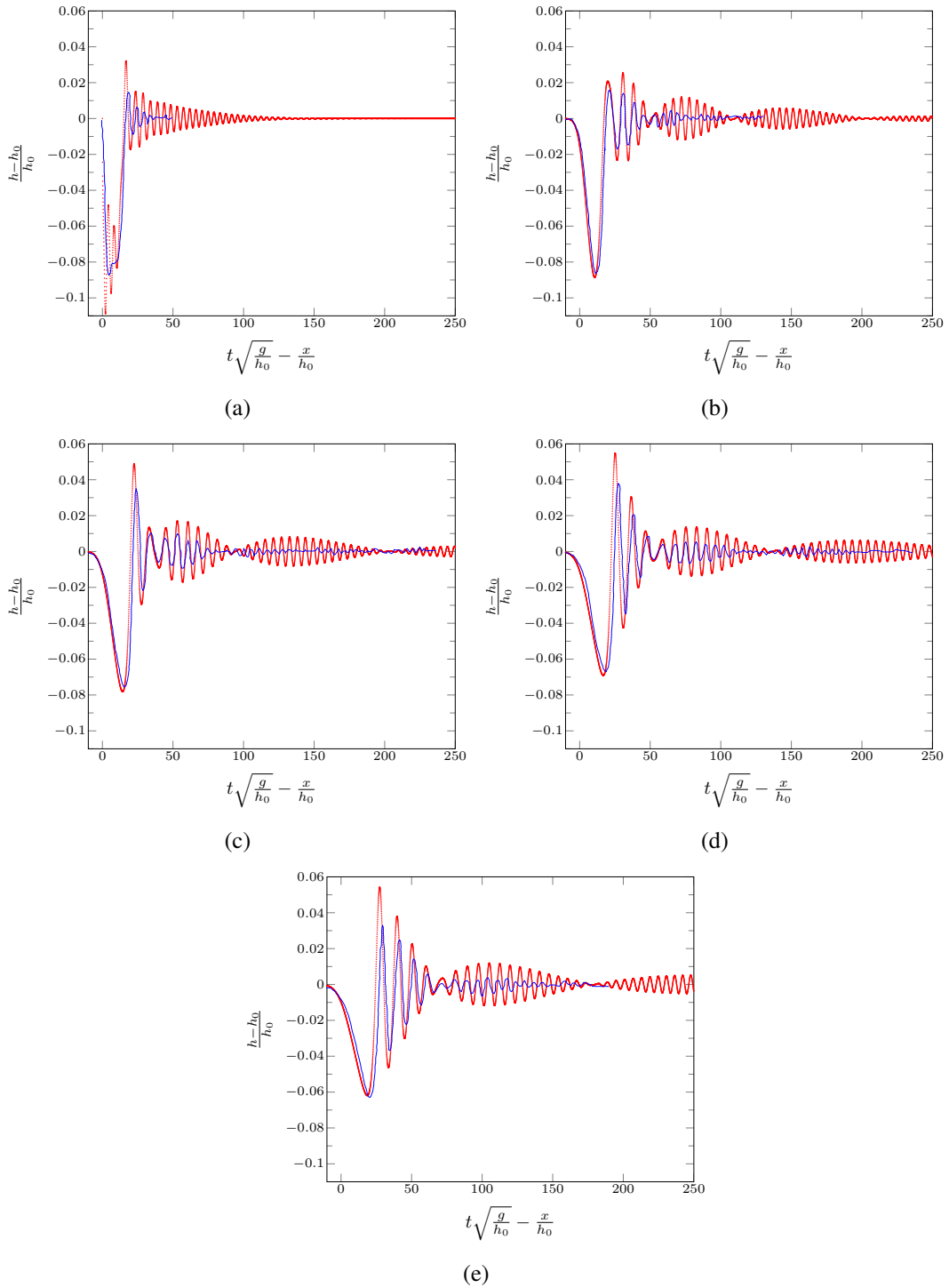


FIG. 6: Comparison of the experimental results (—) against the third-order methods solution (●) at x/h_0 : (a) 0, (b) 50, (c) 100, (d) 150 and (e) 200.

351 **Dam-Break**

352 The dam-break problem used by El et al. (2006) to compare their analysis with a
 353 second-order accurate solution of the Serre equations can be defined by

$$354 \quad h(x, 0) = \begin{cases} 1.8m & x < 500m \\ 1.0m & x \geq 500m \end{cases},$$

355 $u(x, 0) = 0.0m/s.$

356 With $x \in [0m, 1000m]$ for $t \in [0s, 30s]$. Where $\Delta t = 0.5\Delta x / \sqrt{gh_1}$ which satisfies (8)
 357 and $\theta = 1.2$ for the second-order scheme. This corresponds to sub-critical flow and was
 358 a situation demonstrated in El et al. (2006) and Le Métayer et al. (2010). An example
 359 was plotted for $\Delta x = 100/2^{11}m$ for all the methods and for $\Delta x = 100/2^{17}m$ for the first-
 360 order method in Figure 8. To determine if the oscillations that occur in the solution indeed
 361 converge to some limit as $\Delta x \rightarrow 0$ multiple Δx values were run and then the amount of
 362 variation in the solution measured. This measured how oscillatory the solution was and
 363 was used to determine the growth of the oscillations. A common way to measure this is
 364 the total variation (TV) which for q is given by

$$365 \quad TV(q) = \sum_{\forall i > 1} |q_i - q_{i-1}|.$$

366

367 If the solution does indeed converge then the TV must at some point plateau, bounding
 368 the oscillations. This was indeed the findings of the experiments as can be seen by Fig-
 369 ure 7. The TV increases as Δx decreased because the models resolved more dispersive
 370 waves. As Δx decreased further the TV plateaued and so the size and number of oscilla-
 371 tions was bounded. Therefore, the method has not become unstable which supports the
 372 argument that the numerical methods do not introduce non-physical oscillations in the so-
 373 lution. Under this measure the second-order method converges rapidly to the solution of
 374 the third-order method.

375 These solutions compare very well to the findings in El et al. (2006) with both the
 376 second- and third-order methods resolving the oscillations around the “contact discontinuity”(El et al. 2006) between the rarefaction fan and the shock. In Le Métayer et al. (2010)
 377 it was reported that for their first-order method such oscillatory behaviour was not seen.
 378 However, for the first-order method proposed in this paper when $\Delta x = 100/2^{15}$ it was
 379 resolved as in Figure 8(d). This validates the findings in El et al. (2006). Interestingly this
 380 is a much higher resolution than one needs to represent the waves themselves. It appears
 381 that the behaviour of the dispersive waves around a steep gradient is sensitive to diffusion
 382 so that even though the first-order method in Figure 8(a) heuristically had enough cells to
 383 resolve most of the wave train, due to strong diffusion hardly any of the wave train was
 384 resolved.

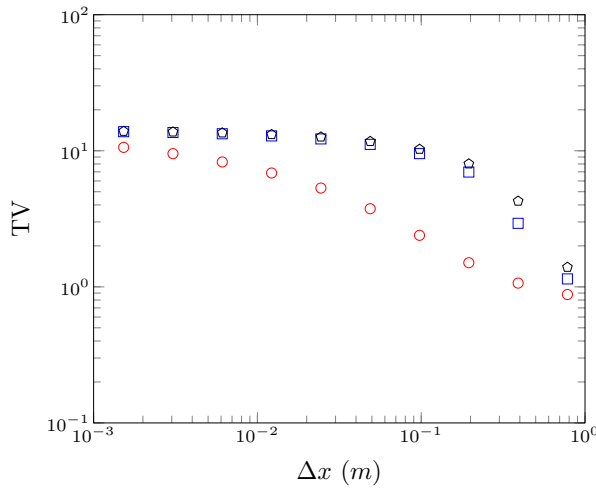


FIG. 7: The change in total variation (TV) of h over Δx for: (○) first-, (□) second-, and (*) third-order methods.

386 There is a good agreement between the second- and third-order simulations of the dam-
 387 break problem as can be seen in Figures 8(b) and 8(c). Although more oscillations are
 388 resolved by the third-order method over the second-order method, there is no significant
 389 change in the resolved behaviour of this problem between the two methods. As noted in the
 390 introduction second-order accurate numerical schemes are dissipative; since the diffusive
 391 third-order method resolved the same oscillations it was demonstrated that none of the
 392 dissipative errors significantly polluted the wave train and for this problem the second-
 393 order accurate scheme is capable of resolving the problem.

394 CONCLUSIONS

395 First-, second- and third-order hybrid finite difference-volume methods were devel-
 396 oped to solve the Serre equations written in conservative law form. The methods were
 397 then tested and validated. Firstly the order of the methods were all verified, secondly
 398 the methods steep gradient handling capability was validated by comparison with experi-
 399 mental data. Thirdly the behaviour of the solutions matched previous findings in El et al.
 400 (2006). Thus it can be concluded that these methods are all valid and they properly handle
 401 steep gradients. It was also demonstrated that for these equations although second-order
 402 is not as accurate as third-order it still provides a satisfactory method for reasonable Δx
 403 unlike the first-order method which due to the introduction of large numerical diffusion
 404 requires computationally restrictive Δx to produce satisfactory accuracy. Therefore; prac-
 405 tical problems which contain steep gradients require at least a second-order method to

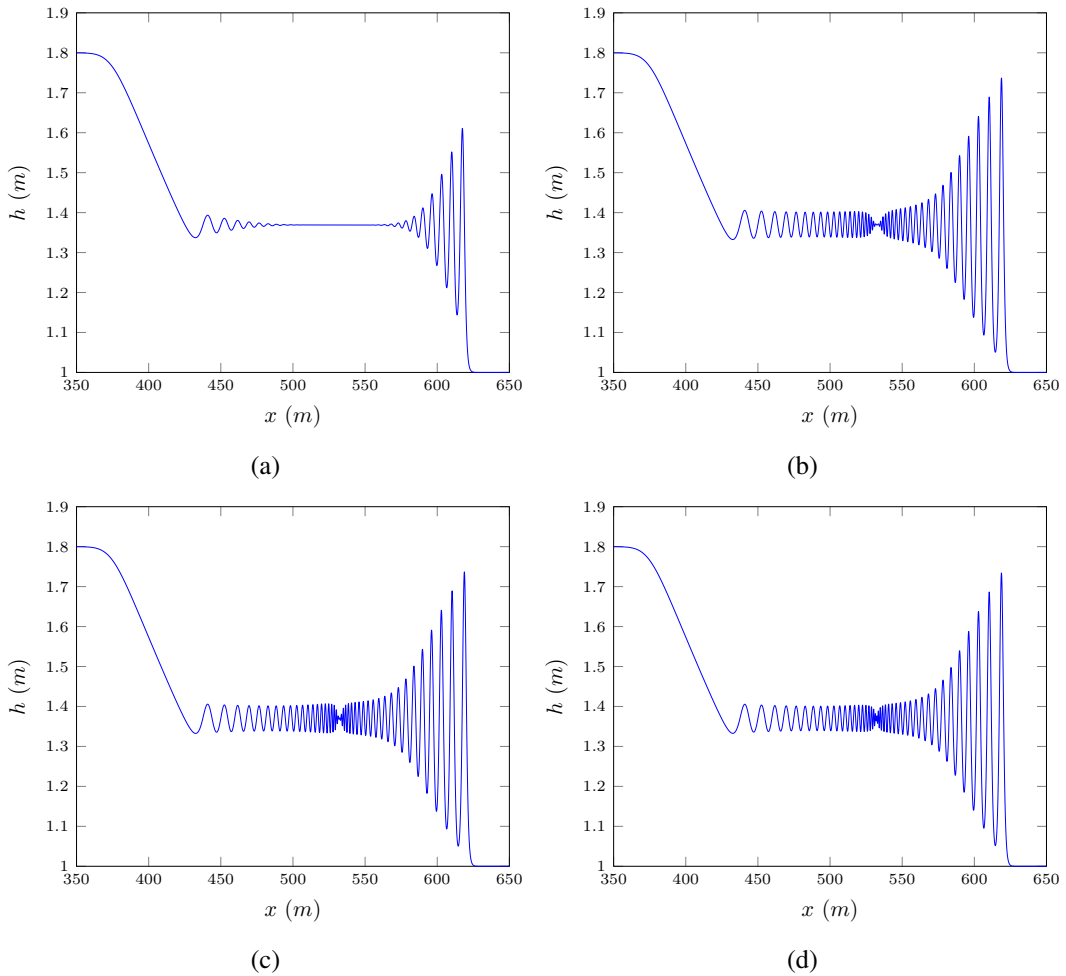


FIG. 8: Solution of the dam-break problem using the (a) first-, (b) second- and (c) third-order method with $\Delta x = 100/2^{11} \text{m}$. As well as a (d) first-order method with $\Delta x = 100/2^{17} \text{m}$.

406 solve the Serre equations.

407 **ACKNOWLEDGEMENTS**

408 Dr David George, Cascades Volcano Observatory, U.S. Geological Survey for providing
409 the rectangular wave data.

410 **REFERENCES**

- 411 Antunes do Carmo, A., Seabra-Santos, F. J., and Almeida, A. B. (1993). “Numerical solution
412 of the generalized Serre equations with the MacCormack finite-difference scheme.” *International Journal for Numerical Methods in Fluids*, 16(8), 725–738.
- 413 Bonneton, P., Chazel, F., Lannes, D., Marche, F., and Tissier, M. (2011). “A splitting approach for the fully nonlinear and weakly dispersive Green-Naghdi model.” *Journal of Computational Physics*, 230(4), 1479–1498.
- 414 Carter, J. D. and Cienfuegos, R. (2011). “Solitary and cnoidal wave solutions of the Serre
415 equations and their stability.” *European Journal of Mechanics B/Fluids*, 30(3), 259–268.
- 416 Chazel, F., Lannes, D., and Marche, F. (2011). “Numerical simulation of strongly nonlinear
417 and dispersive waves using a Green-Naghdi model.” *Journal of Scientific Computing*, 48(1-3), 105–116.
- 418 Cienfuegos, R. and Barthélemy, E. and Bonneton, P. (2006). “A fourth-order compact finite
419 volume scheme for fully nonlinear and weakly dispersive Boussinesq-type equations.
420 Part i: model development and analysis.” *International Journal for Numerical Methods
421 in Fluids*, 51, 1217–1253.
- 422 Cienfuegos, R. and Barthélemy, E. and Bonneton, P. (2007). “A fourth-order compact finite
423 volume scheme for fully nonlinear and weakly dispersive Boussinesq-type equations.
424 Part ii: Boundary conditions and validation.” *International Journal for Numerical
425 Methods in Fluids*, 53, 1423–1455.
- 426 Courant, R., Friedrichs, K., and Lewy, H. (1928). “Über die partiellen Differenzengleichungen
427 der mathematischen physik.” *Mathematische Annalen*, 100(1), 32 – 74.
- 428 Dutykh, D., Clamond, D., Milewski, P., and Mitsotakis, D. (2011). “Finite volume and
429 pseudo-spectral schemes for the fully nonlinear ‘irrotational’ Serre equations.” *Arxiv*,
24(5), 0 – 25.
- 430 El, G., Grimshaw, R. H. J., and Smyth, N. F. (2006). “Unsteady undular bores in fully
431 nonlinear shallow-water theory.” *Physics of Fluids*, 18(027104).
- 432 Godunov, S. K. (1959). “A difference method for numerical calculation of discontinuous
433 solutions of the equations of hydrodynamics.” *Matematicheskii Sbornik*, 89(3), 271–
434 306.
- 435 Gottlieb, S., Ketcheson, D. I., and Shu, C. W. (2009). “High order strong stability preserving
436 time discretizations.” *Journal of Scientific Computing*, 38(3), 251–289.
- 437 Green, A. E. and Naghdi, P. M. (1976). “A derivation of equations for wave propagation
438 in water of variable depth.” *Journal of Fluid Mechanics*, 78(2), 237–246.

- 444 Hammack, J. L. and Segur, H. (1978). “The Korteweg-de Vries equation and water waves.
 445 Part 3. Oscillatory waves.” *Journal of Fluid Mechanics*, 84(2), 337–358.
- 446 Koren, B. (1993). “A robust upwind discretization method for advection, diffusion and
 447 source terms.” *Notes on Numerical Fluid Mechanics*, Vol. 45, Centrum voor Wiskunde
 448 en Informatica, Amsterdam.
- 449 Kurganov, A., Noelle, S., and Petrova, G. (2002). “Semidiscrete central-upwind schemes
 450 for hyperbolic conservation laws and Hamilton-Jacobi equations.” *Journal of Scientific
 451 Computing, Society for Industrial and Applied Mathematics*, 23(3), 707–740.
- 452 Lannes, D. and Bonneton, P. (2009). “*Physics of Fluids*, 21(1), 16601–16610.
- 453 Le Métayer, O., Gavrilyuk, S., and Hank, S. (2010). “A numerical scheme for the Green-
 454 Naghdi model.” *Journal of Computational Physics*, 229(6), 2034–2045.
- 455 Li, M., Guyenne, P., Li, F., and Xu, L. (2014). “High order well-balanced CDG-FE meth-
 456 ods for shallow water waves by a Green-Naghdi model.” *Journal of Computational
 457 Physics*, 257, 169–192.
- 458 Mitsotakis, D., Ilan, B., and Dutykh, D. (2014). “On the Galerkin/Finite-Element Method
 459 for the Serre Equations.” *Journal of Scientific Computing*, 61(1), 166–195.
- 460 Serre, F. (1953). “Contribution à l’étude des écoulements permanents et variables dans les
 461 canaux.” *La Houille Blanche*, 6, 830–872.
- 462 Su, C. H. and Gardner, C. S. (1969). “Korteweg-de Vries equation and generalisations.
 463 III. Derivation of the Korteweg-de Vries equation and Burgers equation.” *Journal of
 464 Mathematical Physics*, 10(3), 536–539.
- 465 Zoppou, C. (2014). “Numerical solution of the One-dimensional and Cylindrical Serre
 466 Equations for Rapidly Varying Free Surface Flows.” Ph.D. thesis, Australian National
 467 University, Acton ACT 2601 Australia.
- 468 Zoppou, C. and Roberts, S. (1996). “Behaviour of finite difference schemes for advection
 469 diffusion equations.” *Technical Report Mathematics Research Report No.MRR 062-96*.